

Angular motion point spread function model considering aberrations and defocus effects

Iftach Klapp and Yitzhak Yitzhaky

Department of Electro-Optics Engineering, Ben Gurion University, Beer Sheva 84105, P.O. Box 653, Israel

Received August 19, 2005; revised December 14, 2005; accepted December 16, 2005; posted March 17, 2006 (Doc. ID 64203)

When motion blur is considered, the optics point spread function (PSF) is conventionally assumed to be fixed, and therefore cascading of the motion optical transfer function (OTF) with the optics OTF is allowed. However, in angular motion conditions, the image is distorted by space-variant effects of wavefront aberrations, defocus, and motion blur. The proposed model considers these effects and formulates a combined space-variant PSF obtained from the angle-dependent optics PSF and the motion PSF that acts as a weighting function. Results of comparison of the new angular-motion-dependent PSF and the traditional PSF show significant differences. To simplify the proposed model, an efficient approximation is suggested and evaluated. © 2006 Optical Society of America

OCIS codes: 080.1010, 110.0110, 110.4850.

1. INTRODUCTION

Angular motion is very common in moving imaging systems such as systems mounted on vehicles (cars, ships, planes, etc.), home video, robot vision, and so on. Extensive research has been done regarding the point spread function (PSF) [or its Fourier transform, the optical transfer function (OTF)] of motion.^{1–10} Nevertheless, the effects of the motion on the OTF of the optics have been treated separately from that of the optics itself. According to the traditional system OTF approach,³ on its course from the object plane to the image plane, the optical wavefront may go through several disturbing media or processes (such as an atmospheric path, motion, optics, imager, etc.). The traditional OTF approach of system engineering analysis describes the influence of each stage by its OTF (assuming a linear space-invariant system) and then calculates the overall system OTF as the product of all the stages' OTFs (cascade). This method has an important advantage of enabling the designer to analyze the influence of each stage on the overall image quality independently.

The traditional cascade approach assumes a space- and time-invariant system, allowing a single PSF across the entire field of view (FOV). The PSF may be calculated at several points across the FOV. However, when the effect of motion blur is considered, authors tend to assume space-invariant optics for simplification.³ In this case the PSF is calculated at the central field point (the optical axis) and is assumed to represent the entire FOV. When the optics is assumed to be space invariant in this approach, its PSF for each object location does not change in time when motion occurs, allowing simpler, but less accurate PSF calculation.

The accuracy of the combined space-invariant OTF of both angular motion and optics attained by cascading (multiplying) approximated motion and optics OTFs appears to suffer for the following reasons:

1. When a fixed object point is imaged during angular motion, the optics PSF is time-space varying due to the

changes of the object distance that result from the changes of viewing angle during exposure (space-variant defocus). This is significant when the object movement is greater than the depth of field of the optical system.

2. In the presence of aberrations, the motion-induced optics PSF is not identical across the entire FOV. Each field point has a different optics PSF depending on the viewing angle (space-variant aberrations).

3. Even in the absence of aberrations, the same angular motion will cause different displacement (blurs) on the imager for points at different angular locations on the object plane (space-variant motion).

This paper proposes a more accurate model, which includes both the space-variant nature of the imaging system and the dynamic effects of the angular motion to determine the combined optics and motion PSF for different locations in the FOV. The space-variant PSF is developed by analyzing two types of wavefront error causes: defocus and *Seidel* aberrations (which include spherical, astigmatism, field curvature, distortion, and coma). In the new model, the motion PSF is used as a weighting function for the local optics PSF that varies during the exposure.

2. INFLUENCE OF ANGULAR MOTION ON THE WAVEFRONT ERRORS

In the following analysis, we assume for simplicity that throughout the integration time the shutter is wide open and the imager's distance from the lens vertex does not change. In contrast, the relative angular motion between the optical system and a static object point, or the viewing angle, is continuously changing. Two types of wavefront errors caused by the varying viewing angle are considered:

1. "Dynamic aberration errors," which result from the change in the relative amount of wavefront aberrations depending on the angular location of the object point.

2. “Dynamic defocus,” which results from the change of the image focal location while the physical distance between the imager and the lens vertex is fixed. This dynamic defocus will be expressed here in terms of wavefront error.

Angular motion analysis setup. Figure 1 describes four states (1–4) of angular motion around a single axis. Two object points (on and off the optical axis) are imaged. State 2 is the center of rotation, where the on-axis object point is aligned with the optical axis. In this state the two points are on the same paraxial object plane and are focused at the sensor (the image plane). Due to the rotation of the camera (around the thin lens center), the physical object and image planes will no longer satisfy the paraxial optics conditions. For each point we define new object and image planes that are perpendicular to the rotated optical axis and satisfy the paraxial optics approximation approach for the point. In Fig. 1 the single paraxial plane system (Obj Pln0/Imager) will separate due to the angular rotations into two new paraxial plane systems (Obj Pln1/Img Pln1 and Obj Pln2/Img Pln2). The new planes are used for the calculation of the aberrations at that temporal angular state. The dynamic distance between the new temporary paraxial image plane and the imager sig-

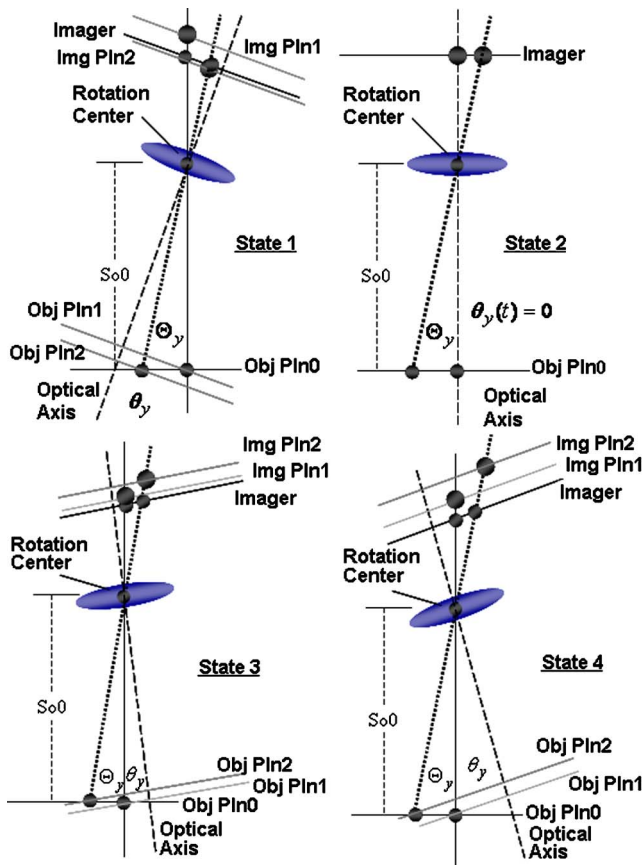


Fig. 1. (Color online) Four representative states (1–4) of a rotation around a single axis. The physical object and image planes are marked “Obj Pln0” and “Imager,” respectively. Paraxial object and image planes due to the angular motion are marked “Obj Pln1” and “Obj Pln2,” and “Img pln1” and “Img pln2,” respectively. In state 2 the motion angle is 0 deg, and the two object points lie in the same (physical) object plane.

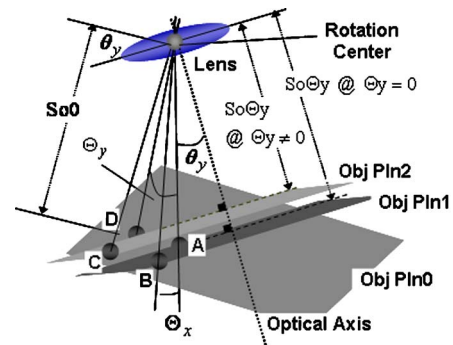


Fig. 2. (Color online) Representative object point locations and corresponding paraxial object planes: point $A(\Theta_x=0, \Theta_y=0)$ is an on-axis point, point $B(\Theta_x=2.5, \Theta_y=0)$ is off axis perpendicular to the motion direction, point $C(\Theta_x=2.5, \Theta_y=2.5)$ is off axis in the two directions, and point $D(\Theta_x=0, \Theta_y=2.5)$ is off axis in the motion direction.

nifies the dynamic defocus. The images of each object point are marked in each step on both the imager and the paraxial image plane. The profile of the image of the point on the imager during the exposure (the PSF) will be analyzed below. In the development of the model, we assume for simplicity an angular motion around the y axis only.

Figure 2 determines four representative object point locations (relative to the optical axis) as follows: point $A(\Theta_x=0, \Theta_y=0)$ is an on-axis point, point $B(\Theta_x \neq 0, \Theta_y=0)$ is off axis perpendicular to the motion direction, point $C(\Theta_x \neq 0, \Theta_y \neq 0)$ is off axis in both directions, and point $D(\Theta_x=0, \Theta_y \neq 0)$ is off axis in only the motion direction.

3. DEFOCUS AND ABERRATION WAVEFRONT ERROR

A. Image Location during Angular Motion

The result of motion during the integration time is image blur in the motion direction. The overall space-variant blur is determined by both motion and optics PSFs. We can describe this blur as a summation or integration of the instantaneous optics PSFs (denoted PSF_{opt}) over the exposure. The contribution of each instantaneous PSF_{opt} depends on its location, shape, and weight in the overall summation. The weight is proportional to time spent at this location according to the motion PSF. Figure 3 presents the geometry of an instantaneous imaging state of a point $P_0(X_0, Y_0)$. The angular motion measured relative to an initial optical axis location (state 2) is indicated by $\theta_y(t)$, and the angular location of the object point in the x and y directions is (Θ_x, Θ_y) . The coordinates of the image point $P_1(X_1, Y_1)$ at time t will be

$$X_1 = Si_0 \tan[\theta_y(t) - \Theta_y], \tag{1}$$

$$Y_1 = \{Si_0/\cos[\theta_y(t) - \Theta_y]\}\tan[\theta_x(t) - \Theta_x]. \tag{2}$$

Assuming rotation around the y axis only [$\theta_x(t)=0$], we get

$$Y_1 = \{Si_0/\cos[\theta_y(t) - \Theta_y]\}\tan(-\Theta_x), \tag{3}$$

where Si_0 is the nominal (physical) image plane distance and $Si_0/\cos[\theta_y(t) - \Theta_y]$ is the distance from the center of rotation to the image point [symbolized by $R(t)$ in Fig. 3].

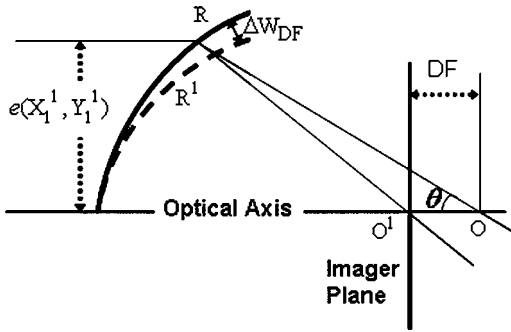


Fig. 4. Defocus wavefront representation. R and R^1 are perfect and reference wavefronts, with centers at O and O^1 , respectively. DF and ΔW_{DF} are defined as the defocus and the defocus wavefront error, respectively.

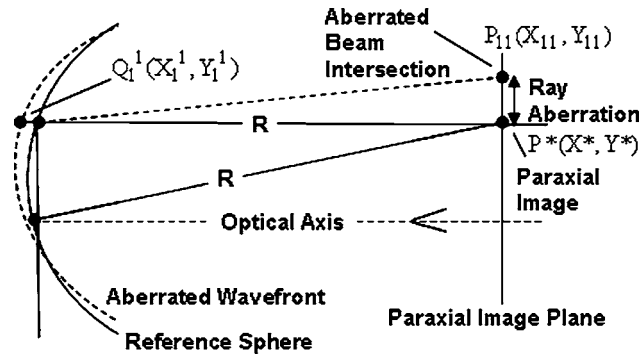


Fig. 5. Illustration of a cross section of a nonideal wavefront and a reference sphere forming ray aberration. $P^*(X^*, Y^*)$ is the paraxial image point where the ideal wavefront should converge (ray R), and $P_{11}(X_{11}, Y_{11})$ is the intersecting point of an aberrated ray $Q_1^1 P_{11}$. The distance between the two points is the ray aberration.

$$\Delta W_{DF} = -\frac{1}{2}n_1 \frac{e^2}{R^2} DF(\theta_y(t), \Theta_x, \Theta_y). \quad (12)$$

2. Aberration-Induced Wavefront Errors

Optical imaging systems do not form perfect images. A nonperfect lens causes various wavefront aberrations that may result in an image of a point expanding beyond the size of the diffraction-limited PSF.¹² The wavefront error in this case can be described by Seidel aberrations.¹³ Assuming a rotationally symmetric system, the aberration wavefront error in the exit pupil plane can be formulated as¹³

$$\phi^{(4)} = -\frac{1}{4}B\rho^4 - Ck^4 - \frac{1}{2}Dr^2\rho^2 + Er^2k^2 + F\rho^2k^2, \quad (13)$$

where B , C , D , E , and F are the Seidel aberration coefficients corresponding, respectively, to the fourth-order aberrations (also commonly known as *third-order* aberrations): spherical, astigmatism, field curvature, distortion, and coma.

To explain the rest of the arguments of Eq. (13), we will first determine the wavefront propagation in the imaging system. We can imagine a cone of rays leaving an object point toward the entrance pupil of the optical system. A conjugate cone of rays will then leave the exit pupil. As illustrated in Fig. 5 for a single ray, each ray of that out-

put cone passes through a specific coordinate in the exit pupil, (X_1^1, Y_1^1) , and strikes the paraxial image plane at point (X_{11}, Y_{11}) near the paraxial image point (X^*, Y^*) . For convenience, we can transform the coordinates of the object plane, the exit pupil plane, and the paraxial image plane into new units of length called Seidel variables,¹³ as shown in Table 1.

In this table γ_0 and γ_1 are units of length of the entrance and exit pupils, respectively, such that the lateral magnification between the planes of the entrance and the exit pupil, $M' = \gamma_1/\gamma_0$, is assumed to be 1 (as a single thin lens is assumed here), n_0 and n_1 are the refractive indices in the object and the image space, and k , ρ , and r are the fourth-power combinations of Seidel variables:

$$k^2 = x_0\xi_1 + y_0\eta_1, \quad \rho^2 = \xi_1^2 + \eta_1^2, \quad r^2 = x_0^2 + y_0^2. \quad (14)$$

From the wavefront error equation (13), it is clear that the wavefront error due to the aberrations highly depends on the ray angle (expressed as angular distance between the object point and the optical axis). Thus, in an aberrated optical system, the angular motion will cause continuous changes in wavefront errors, termed here dynamic wavefront aberrations. It should be noted that a consideration of higher-order aberrations as well will increase the accuracy of the model.

3. Overall Wavefront Error via Ray Aberration Calculations

The overall wavefront error is obtained by summing the dynamic defocus wavefront error and the aberration wavefront error. The wavefront error function is the local optical path difference of the true wavefront relative to a pure sphere. A derivative of that error function will be the error in the ray direction that is associated with that location and ideally points to the center of the ideal sphere. Multiplication of the ray direction error by the image distance produces the relative offset of the ray, called ray aberration. The derivative of Eq. (13) in both directions produces the horizontal and vertical components of the ray aberration angle relative to the paraxial ray direction¹³

$$\Delta x^{(3)} = x_0(2Ck^2 - Er^2 - F\rho^2) + \xi_1(B\rho^2 + Dr^2 - 2Fk^2), \quad (15)$$

$$\Delta y^{(3)} = y_0(2Ck^2 - Er^2 - F\rho^2) + \eta_1(B\rho^2 + Dr^2 - 2Fk^2). \quad (16)$$

The shift from the paraxial image point of each ray can be calculated by translating back the Seidel coefficients. The

Table 1. Seidel Variables

Object Plane	Image Plane	Exit Pupil
$x_0 = \frac{n_0\gamma_0}{S_{00}}X_0$	$x_1 = \frac{n_1\gamma_1}{S_{10}}X_{11}$	$\xi_1 = \frac{X_1^1}{\gamma_1}$
$y_0 = \frac{n_0\gamma_0}{S_{00}}Y_0$	$y_1 = \frac{n_1\gamma_1}{S_{10}}Y_{11}$	$\eta_1 = \frac{Y_1^1}{\gamma_1}$

ray aberration in the paraxial image plane will be, in each direction,¹³

$$\begin{aligned}\Delta X_{\text{ABR}} &= X_{11} - X^* = \frac{\text{Si}0\Delta x^{(3)}}{n_1\lambda_1}, \\ \Delta Y_{\text{ABR}} &= Y_{11} - Y^* = \frac{\text{Si}0\Delta y^{(3)}}{n_1\lambda_1},\end{aligned}\quad (17)$$

where $P^*(X^*, Y^*)$ is the intersecting point of the paraxial image plane and the ray striking the imager at $P_1(X_1, Y_1)$ (Fig. 3). Since Si0 is the distance to the imager's plane, which can be somewhat shifted from the paraxial plane (as a result of the defocus), X_{11} is actually measured at the imager plane; thus, in practice, $\Delta X_{\text{ABR}} = X_{11} - X_1$ and $\Delta Y_{\text{ABR}} = Y_{11} - Y_1$.

The horizontal and vertical ray aberration components of the defocus contribution can be obtained by differentiating Eq. (12) and multiplying it by Si0:

$$\begin{aligned}\Delta X_{\text{DF}} &= -n_1 \frac{X_1^1}{\text{Si}0} \text{DF}(\theta_y(t), \Theta_x, \Theta_y), \\ \Delta Y_{\text{DF}} &= -n_1 \frac{Y_1^1}{\text{Si}0} \text{DF}(\theta_y(t), \Theta_x, \Theta_y).\end{aligned}\quad (18)$$

The overall wavefront error is obtained by summing the dynamic defocus and aberration wavefront errors:

$$\begin{aligned}\Delta X &= \Delta X_{\text{ABR}} + \Delta X_{\text{DF}}, \\ \Delta Y &= \Delta Y_{\text{ABR}} + \Delta Y_{\text{DF}}.\end{aligned}\quad (19)$$

4. FORMATION OF THE SPACE-VARIANT ANGULAR MOTION POINT SPREAD FUNCTION

The distribution of wavefront error at the exit pupil expresses here both defocus and Seidel aberrations. If it is represented as a phase distribution at the exit pupil, the optics PSF could be calculated with the physical optics approach.^{14,15} However, when the wavefront aberration extent is at least two wavelengths (as assumed here), diffraction can be neglected and a geometrical approach¹⁴ can be used to approximate the local optics OTF as follows:

The spreading rays from the exit pupil intersect the image plane at different locations (ray aberrations). The PSF can be built from the distribution of those intersection points in the image plane. The shape of the PSF is determined by the number of rays striking each area¹⁶ (assuming a uniform ray distribution entering the exit pupil).¹⁷ The instantaneous optics PSF can be approximated by

$$\begin{aligned}\text{PSF}_{\text{opt}}(X_{\text{im}}, Y_{\text{im}}, X_1, Y_1) &= \frac{1}{N} \sum_{i=1}^N \delta\{X_{\text{im}} - [X_1 + \Delta X_i(\psi)], \\ &Y_{\text{im}} - [Y_1 + \Delta Y_i(\psi)]\},\end{aligned}\quad (20)$$

where $(X_{\text{im}}, Y_{\text{im}})$ are the imager coordinates, (X_1, Y_1) are the ideal image coordinates defined in Eqs. (1)–(3), N is

the total number of rays, $(\Delta X_i, \Delta Y_i)$ are determined by the ray aberrations, and ψ symbolizes the parameters on which the ray aberrations depend ($B, C, D, E, F, \text{DF}, \text{Si}0, n_1, n_2, k, r,$ and ρ). The values of these parameters are affected by the relative initial object location (Θ_x, Θ_y) and by the dynamic viewing angle $(\theta_x(t), \theta_y(t))$. In a rotation around the y axis only, $\theta_x = 0$.

A. Angular Motion Point Spread Function

The PSF of the motion during integration is proportional to the inverse of the relative velocity between the imager and the object. This PSF is actually similar to the PDF or the normalized histogram of the motion (represented as location versus time).² If the optics PSF were space invariant during the angular motion, the overall PSF would be a convolution of the optics and motion PSFs. However, as we stated earlier, this relatively simple formation of the angular motion PSF is not accurate because the optics PSF is actually space variant in angular motion conditions. Each viewing angle interval has a corresponding optics PSF, while the fraction of energy imaged from the object at that interval is proportional to the motion PSF value there. Therefore the motion PSF can be employed as the weighting function to the local optics PSF in the exposure process. Mathematically, we can break down the motion PSF into a series of delta functions with different heights, where each delta expresses the portion of energy transferred to each location due to the motion profile:

$$\begin{aligned}\text{PSF}_{\text{motion}}(X_{\text{im}}, Y_{\text{im}}, X_{1i}, Y_{1i}) &= \sum_{i=i_s}^{j_{se}} \text{AMP}_{\text{motion}}(X_{1i}, Y_{1i}) \delta\{X_{\text{im}} \\ &- X_{1i}, Y_{\text{im}} - Y_{1i}\},\end{aligned}\quad (21)$$

where (X_{1i}, Y_{1i}) are discrete image coordinates. The motion range is defined by i_s and i_{se} , where (X_{1i_s}, Y_{1i_s}) and $(X_{1i_{se}}, Y_{1i_{se}})$ represent, respectively, the initial and final image point locations due to the motion process. $\text{AMP}_{\text{motion}}(X_{1i}, Y_{1i})$ is the value of the discrete histogram of the motion at spatial location (X_{1i}, Y_{1i}) . Although the angular motion function $\theta_y(t)$ is similar over the entire imager's FOV, the PSF depends on the position (Θ_x, Θ_y) of the object point, even in the absence of aberrations.

A local PSF is defined as the local optics PSF (PSF_{opt}) weighted by the local motion PSF value $\text{AMP}_{\text{motion}}$:

$$\begin{aligned}\text{PSF}_{\text{local}}(X_{\text{im}}, Y_{\text{im}}, X_{1i}, Y_{1i}) \\ = \text{PSF}_{\text{opt}}(X_{\text{im}}, Y_{\text{im}}, X_{1i}, Y_{1i}) \text{AMP}_{\text{motion}}(X_{1i}, Y_{1i}).\end{aligned}\quad (22)$$

The overall angular motion PSF ($\text{PSF}_{\text{ang motion}}$) is an integration of the point spread distributions in all the locations during the exposure:

$$\begin{aligned}\text{PSF}_{\text{ang motion}}(X_{\text{im}}, Y_{\text{im}}, X_{1i}, Y_{1i}) \\ = \sum_{i=i_s}^{j_{se}} \text{PSF}_{\text{local}}(X_{\text{im}}, Y_{\text{im}}, X_{1i}, Y_{1i}) \otimes \delta\{X_{\text{im}} - X_{1i}, Y_{\text{im}} - Y_{1i}\}.\end{aligned}\quad (23)$$

B. Optical Transfer Function Model

The Fourier transform of the PSF, known as the OTF, can be used in a space-invariant system where the recorded

image is modeled as a convolution between the input image and the PSF (a multiplication in the frequency domain). In the more accurate space-variant model proposed here, a “local OTF” (the Fourier transform of the local PSF) is developed and used to evaluate and compare the system’s response in the spatial frequency domain. A local OTF may be used in a block-based processing, where a *single* OTF is approximated for each block (according to the Fourier transform of the PSF at the center of the block).

The angular motion OTF at location (X_{1i}, Y_{1i}) is the Fourier transform of Eq. (23):

$$\begin{aligned} \text{OTF}_{\text{ang motion}}(\omega_x, \omega_y, X_{1i}, Y_{1i}) \\ = \int \int \sum_{i=i_s}^{i_{se}} [\text{PSF}_{\text{local}}(X_{\text{im}}, Y_{\text{im}}, X_{1i}, Y_{1i}) \\ \otimes \delta(X_{\text{im}} - X_{1i}, Y_{\text{im}} - Y_{1i})] \Omega dX_{\text{im}} dY_{\text{im}}, \end{aligned} \quad (24)$$

where $\Omega = \exp[-j(\omega_x X_{\text{im}} + \omega_y Y_{\text{im}})]$ and (ω_x, ω_y) are the spatial frequency coordinates in the image plane. Exchanging the locations of the summation and the integration yields

$$\begin{aligned} \text{OTF}_{\text{ang motion}}(\omega_x, \omega_y, X_{1i}, Y_{1i}) \\ = \sum_{i=i_s}^{i_{se}} \int \int \text{PSF}_{\text{local}}(X_{\text{im}}, Y_{\text{im}}, X_{1i}, Y_{1i}) \\ \otimes \delta(X_{\text{im}} - X_{1i}, Y_{\text{im}} - Y_{1i}) \Omega dX_{\text{im}} dY_{\text{im}}. \end{aligned} \quad (25)$$

Converting the spatial convolution into a multiplication in the Fourier domain, where $\text{OTF}_{\text{local}}$ is the Fourier transform of $\text{PSF}_{\text{local}}$, produces

$$\begin{aligned} \text{OTF}_{\text{ang motion}}(\omega_x, \omega_y, X_{1i}, Y_{1i}) \\ = \sum_{i=i_s}^{i_{se}} \text{OTF}_{\text{local}}(\omega_x, \omega_y, X_{1i}, Y_{1i}) \times \exp[j(\omega_x X_{\text{im}} + \omega_y Y_{\text{im}})], \end{aligned} \quad (26)$$

where the local OTF ($\text{OTF}_{\text{local}}$) is, according to Eq. (22),

$$\begin{aligned} \text{OTF}_{\text{local}}(\omega_x, \omega_y, X_{1i}, Y_{1i}) \\ = \text{AMP}_{\text{motion}}(X_{1i}, Y_{1i}) \text{OTF}_{\text{opt}}(\omega_x, \omega_y, X_{1i}, Y_{1i}). \end{aligned} \quad (27)$$

5. GENERALIZATION TO OTHER CASES OF MOTION-DEPENDENT OPTICS POINT SPREAD FUNCTION

The proposed model can be used in other cases in which the optics PSF is varying due to motion. Such a case is the time-varying defocus due to motion during exposure perpendicular to the image plane.¹⁸ In this case the optics PSF is a function of a constant aberration form and a varying motion-induced defocus. Here again, the motion PSF can be used as a weighting function for the instantaneous optics PSF, resulting in an OTF of the form

$$\begin{aligned} \text{OTF}_{\text{perp motion}}(\omega_x, \omega_y) \\ = \sum_{i=i_s}^{i_{se}} \text{AMP}_{\text{motion}}[\text{DF}(i)] \text{OTF}_{\text{opt}}[\omega_x, \omega_y, \text{DF}(i)]. \end{aligned} \quad (28)$$

6. SIMULATION SETUP

A thin lens model was used, and a motion around the y axis at the center of the lens was assumed. The motion type was chosen arbitrarily to be a high frequency sinusoidal (in which the exposure equals the temporal sinusoid period multiplied by an integer, or much higher than the period). The motion amplitude was set to be $5 \mu\text{m}$ ($10 \mu\text{m}$ peak-to-peak extent). The optical setup of the simulation is presented in Table 2. The resulting optics PSFs were verified with the OSLO simulator.^{19,20}

7. RESULTS

A. Motion-Only and Optics-Only Modulation Transfer Functions

Although the angular motion function $\theta_y(t)$ is similar for the entire imager FOV, the motion PSF depends on the location of the object point at the object plane, (Θ_x, Θ_y) . Figure 6(a) presents motion-only modulation transfer functions (MTFs) for different initial object point locations ($\Theta_y = 0, 2.5, 10, \text{ and } 15 \text{ deg}$), where the motion function is $\theta_y(t) = 0.057 \sin(2\pi t) \text{ deg}$ and $\text{Si}0 = 47.8 \text{ mm}$. As the angular location of the point increases, the motion PSF extent also increases and the corresponding MTF becomes narrower. Figure 6(b) compares cross sections of optics-only MTFs for the four point locations (A, B, C, and D, as defined in Fig. 2). It can be seen that different point angular locations cause different MTFs.

B. Combined Motion and Optics Effects in Angular Motion

This subsection presents a comparison of PSF and MTF results, obtained by using the traditional and proposed methods, for four representative point locations (A, B, C, and D, as defined in Fig. 2). Although the common high frequency sinusoidal motion type was arbitrarily used in the simulation, other motion types give qualitatively similar results.

Three models have been compared:

Table 2. Optical Setup Used in the Simulation with a Single Thin Lens^a

Parameter	Value	Unit
So0 (Initial object distance)	100	m
Si0 (focal length) ^b	48.37	mm
Entrance diameter	10	mm
Entrance pupil distance	0	mm
Lens front radii	50	mm
Lens back radii	-50	mm
Glass material	BK7	
Electromagnetic wavelength	0.5875	μm
Refractive index	1.5168	

^aThe geometric values and the glass material represent a common optical system. A wavelength of $0.5875 \mu\text{m}$ is frequently used in visible optical design.^{19,20}

^bThe imager distance criterion was an on-axis minimum root mean square spot size (monochromatic) for the above configuration.

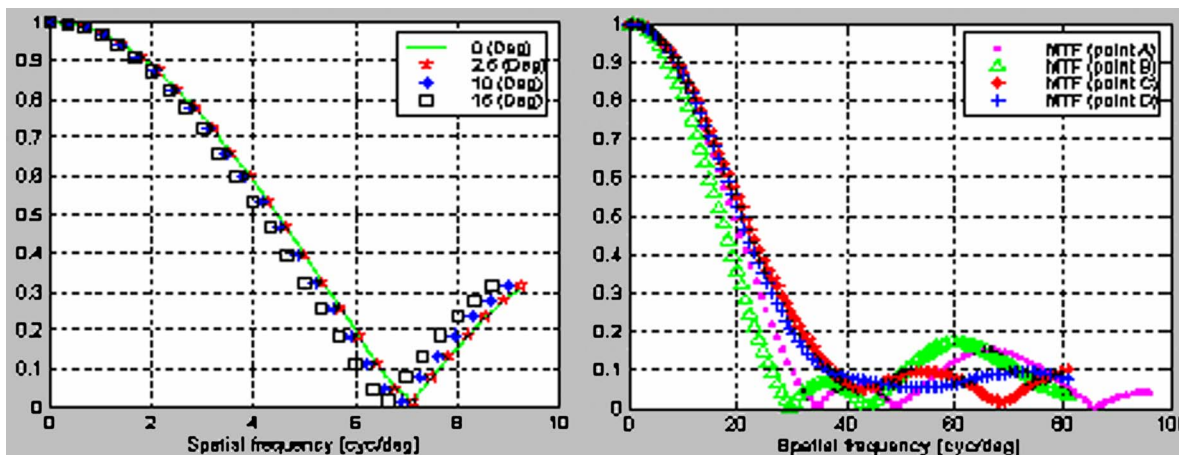


Fig. 6. (Color online) (a) Motion-only (no aberrations) MTFs for different initial object point locations ($\Theta_0=0, 2.5, 10,$ and 15 deg). (b) Comparison of cross sections of optics-only (no motion) MTFs for the four point locations A, B, C, and D, defined in Fig. 2.

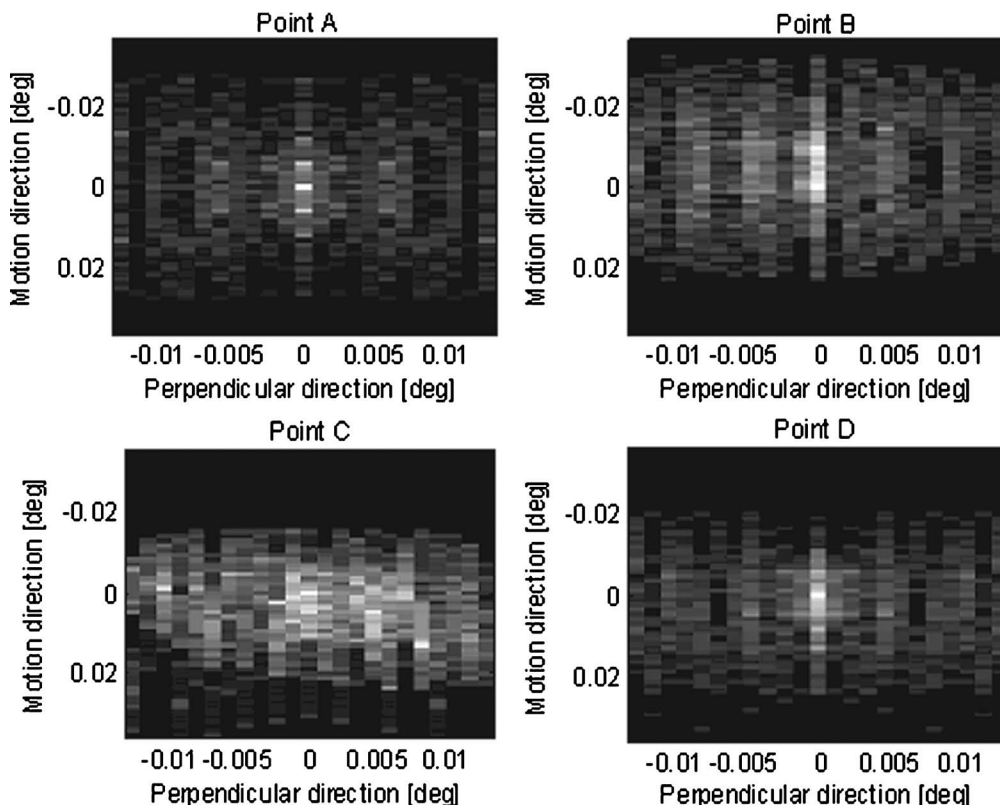


Fig. 7. PSFs of the four representative object points (A, B, C, and D, shown in Fig. 2). Significant differences among the PSFs result from the different locations of the points. In small angular motion (as in this case), the PSF of point A resembles the PSF obtained by the traditional method.

1. The cascade model, in which the on-axis PSF approximation is used and assumed to be space invariant across the FOV of the lens.
2. The proposed model.
3. An approximation of the proposed model, in which motion amplitude is assumed to be much smaller than the lens FOV, enabling a space-invariant optics PSF across the motion range. In this case the optics PSF was approximated according to its value in the center of the motion range.

Figure 7 presents four PSFs of the four points (A, B, C, and D, shown in Fig. 2). Brighter values represent locations where a higher fraction of the intensity of the point is received. The center of each PSF [point (0,0)] is the ideal location of the image of the point when no motion or aberration occurs. It can be seen that significant differences exist among the PSFs as a result of the different locations of the object points. The nonsymmetric natures of the PSFs result from the nonsymmetric nature of the motion-only PSF (that is, one-dimensional) and the differ-

ent locations of the points. A pattern of two peaks separated by the motion extent that can be observed in the PSFs characterizes the PSF of high frequency sinusoidal vibrations. In small angular motion (as in this case), the PSF of point A is similar to its approximated version, which is the same as the traditional PSF.

A common single-number quantitative measure of the image quality limitations imposed by the PSF is the MTFA, which is the area enclosed between the MTF curve and an approximated contrast threshold of the human visual system. Because the PSFs here are not isotropic, the two-dimensional MTF was used, and the contrast threshold was approximated by a constant value of 0.02, which may be considered a rough estimate of the threshold contrast for the human visual system.³ Results are presented in Table 3.

The MTFA values in this table give a quantitative assessment of the image degradation resulting from the PSFs shown in Fig. 7. It can be seen that significantly different MTFA values are obtained for points at different locations under the given setup. Point A (located at the optical axis) suffers the lowest degradation, while point B suffers the highest. The relatively large variations among the MTFA values mean that taking into account the space-variant effects of the angular motion and the object location in the FOV can become significant.

Figure 8(a) compares cross sections (in the motion direction) of the overall angular motion MTFs for the four point locations (A, B, C, and D, shown in Fig. 2) with regard to an approximated contrast threshold of the human

Table 3. Two-Dimensional MTFAs for the PSFs Shown in Fig. 7

Point	2-D MTFA	
A	678	9
B	510	9
C	573	2
D	644	0

eye. Figure 8(b) compares cross sections of the MTFs for point C, obtained by the proposed model, the traditional method, and the approximation of the proposed model. The motion-only and optics-only MTFs of point C are also shown in this figure. The wider motion-only MTF indicates that, in this specific setup, motion amplitude was relatively small and causes smaller image degradation than the optics. The results show significant differences between system MTFs using the new model and system MTFs using the traditional cascade approach. The high similarity between the proposed method and its approximated version is due to the motion magnitude's being much smaller than the lens FOV; thus the approximation of the optics PSF by its value at the center of the motion range is satisfying. As motion amplitude increases, smaller differences appear between the results of the traditional model and those of the new model for the same point because the motion becomes more dominant. However, due to dependency of the motion PSF on the object point location, different object point locations will have different motion-only MTFs.

8. CONCLUSIONS

In this work a new model of the angular motion PSF was developed. The model takes into account the Seidel aberrations and defocus effects, which depend on the angular position of the object (located at the object plane) relative to the optical axis. In motion condition these space-variant optical effects are also time variant (dynamic). Integration of the dynamic Seidel aberrations and defocus with the motion effect during exposure produces a space-variant overall PSF, in which a space-variant optics PSF is integrated along the motion path and weighted according to the motion PSF. This is different from the traditional method when combining motion-blur effects with the optics response, in which the optics PSF is considered space invariant and equals the response at the optical axis. In the case where the motion amplitude is much smaller than the lens FOV, an approximation is proposed

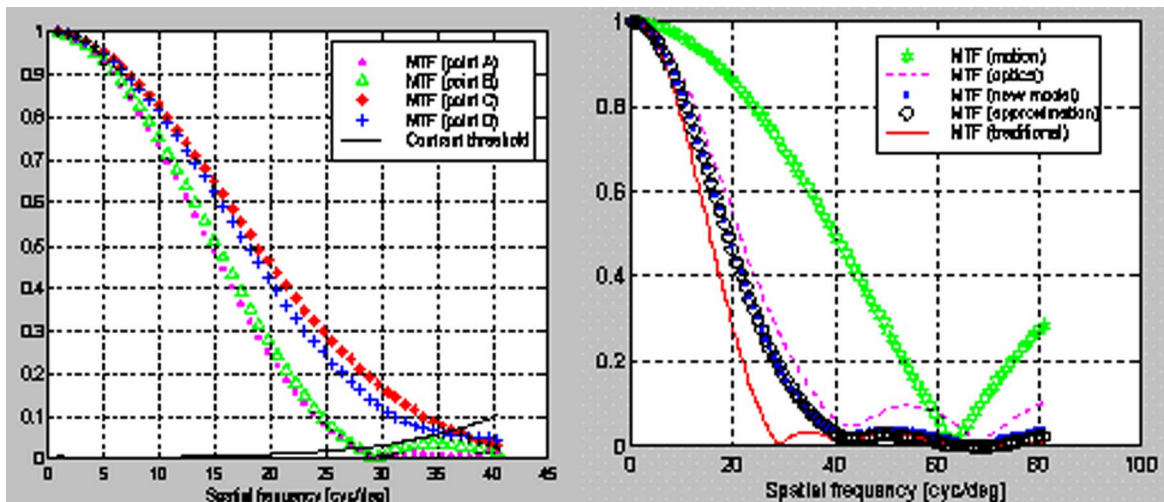


Fig. 8. (Color online) Comparison of cross sections (in the motion direction) of the overall angular motion MTFs for the four point locations (A, B, C, and D, as defined in Fig. 2) with regard to an approximated contrast threshold of the human eye. (b) Comparison of cross sections (in motion direction) of the angular motion MTFs for point C, obtained by the proposed model, the traditional method, and the approximation. The motion only and optics only MTFs of point C are also shown.

in which the optics PSF across the motion range is space invariant, approximated by its value in the center of the motion range. Results of angular motion MTF comparisons of the traditional, proposed, and approximated models show significant differences between the results of the traditional and proposed methods, indicating that neglecting the space-variant properties of the imaging system may cause inaccuracies in MTF calculations. As pointed out in Section 4, the proposed method can be generalized to other cases where the optics PSF is motion dependent, such as a dynamic defocus during motion in the direction of the optical axis.

Author contact information: Yitzhak Yitzhaky (corresponding author), Ben-Gurion University, Department of Electro-Optics Engineering, Beer-Sheva 84105, P.O. Box 653, Israel; e-mail, itzik@ee.bgu.ac.il; phone, 972-8-6461840; fax, 972-8-6479494.

REFERENCES

- O. Hadar, M. Fisher, and N. S. Kopeika, "Image resolution limits resulting from mechanical vibration. Part III: Numerical calculation of modulation transfer function," *Opt. Eng. (Bellingham)* **31**, 581–589 (1992).
- O. Hadar, I. Dror, and N. S. Kopeika, "Image resolution limits resulting from mechanical vibration. Part IV: Real time numerical calculation of optical transfer function and experimental verification," *Opt. Eng. (Bellingham)* **33**, 566–578 (1994).
- N. S. Kopeika, *A System Engineering Approach to Imaging* (SPIE, 1998).
- G. C. Holst, *Electro-Optical Imaging System Performance* (SPIE, 1995), pp. 67–70.
- M. D. Rosenau, "Parabolic image motion," *Photogramm. Eng.* **27**, 421–426 (1961).
- S. Rudoler, O. Hadar, M. Fisher, and N. S. Kopeika, "Image resolution limits resulting from mechanical vibration. Part II: Experiment," *Opt. Eng. (Bellingham)* **30**, 577–589 (1991).
- P. V. Shack, "The influence of image motion and shutter operation on the photographic transfer function," *Appl. Opt.* **3**, 1171–1181 (1964).
- S. C. Som, "Analysis of the effect of linear smear on photographic images," *J. Opt. Soc. Am.* **61**, 859–864 (1971).
- T. Tortt, "The effect of motion on resolution," *Photogramm. Eng.* **26**, 819–827 (1960).
- D. Wuilich and N. S. Kopeika, "Image resolution limits resulting from mechanical vibration," *Opt. Eng. (Bellingham)* **26**, 529–533 (1987).
- H. H. Hopkins, *Wave Theory of Aberrations* (Clarendon, 1950), pp. 10–14, 51–53, 77–87.
- S. G. Lipson and H. L. Lipson, *Optical Physics* (Cambridge U. Press, 1981), pp. 404–407.
- M. Born and E. Wolf, *Principles of Optics*, 6th ed. (Pergamon, 1986), pp. 110–114, 133–140, 186–187, 203–230.
- K. Miyamoto, "Image evaluation by spot diagram using a computer," *Appl. Opt.* **2**, 1247–1250 (1963).
- R. Kingslake, *Lens Design Fundamentals* (Academic, 1978), pp. 152–153.
- K. Miyamoto, "On a comparison between wave optics and geometrical optics by using Fourier analysis. I. General theory," *J. Opt. Soc. Am.* **48**, 57–63 (1958).
- K. Miyamoto, "Comparison between wave optics and geometrical optics using Fourier analysis. II. Astigmatism, coma, spherical aberration," *J. Opt. Soc. Am.* **48**, 567–575 (1958).
- A. W. Lohmann and D. P. Paris, "Influence of longitudinal vibrations on image quality," *Appl. Opt.* **4**, 393–397 (1965).
- OSLO-EDU, version 6.2.2, Help file, "Seidel wavefront" (Lambda Research Corporation, 2003).
- OSLO-EDU, version 6.1, Optics Reference Manual (Lambda Research Corporation, 2001), pp. 113–114.